AIP Applied Physics Letters

3m aperture probes for near-field terahertz transmission microscopy

Alexander J. Macfaden, John L. Reno, Igal Brener, and Oleg Mitrofanov

Citation: Applied Physics Letters **104**, 011110 (2014); doi: 10.1063/1.4861621
View online: http://dx.doi.org/10.1063/1.4861621
View Table of Contents: http://scitation.aip.org/content/aip/journal/apl/104/1?ver=pdfcov
Published by the AIP Publishing

Articles you may be interested in

Quantitative coherent scattering spectra in apertureless terahertz pulse near-field microscopes
Appl. Phys. Lett. **101**, 011109 (2012); 10.1063/1.4733475

Low temperature near-field scanning optical microscopy on infrared and terahertz photonic-crystal quantum cascade lasers
Appl. Phys. Lett. **98**, 231112 (2011); 10.1063/1.3597411

Slit waveguide based terahertz near-field microscopy: Prospects and limitations
J. Appl. Phys. **107**, 033504 (2010); 10.1063/1.3294623

A study of background signals in terahertz apertureless near-field microscopy and their use for scattering-probe imaging
J. Appl. Phys. **105**, 113117 (2009); 10.1063/1.3141727

Waveguide mode imaging and dispersion analysis with terahertz near-field microscopy
Appl. Phys. Lett. **94**, 171104 (2009); 10.1063/1.3126053

This article is copyrighted as indicated in the article. Reuse of AIP content is subject to the terms at: http://scitation.aip.org/termsconditions. Downloaded to IP: 144.82.107.68 On: Tue, 20 May 2014 14:15:49

3 μm aperture probes for near-field terahertz transmission microscopy

Alexander J. Macfaden,[1] John L. Reno,[2,3] Igal Brener,[2,3] and Oleg Mitrofanov[1,2,a)]
[1]*Department of Electronic & Electrical Engineering, UCL, London WC1E 7JE, United Kingdom*
[2]*Center for Integrated Nanotechnologies, Sandia National Laboratories, Albuquerque, New Mexico 87185, USA*
[3]*Sandia National Laboratories, Albuquerque, New Mexico 87185, USA*

(Received 15 November 2013; accepted 19 December 2013; published online 8 January 2014)

The transmission of electromagnetic waves through a sub-wavelength aperture is described by Bethe's theory. This imposes severe limitations on using apertures smaller than ~1/100 of the wavelength for near-field microscopy at terahertz (THz) frequencies. Experimentally, we observe that the transmitted evanescent field within 1 μm of the aperture deviates significantly from the Bethe dependence of $E \propto a^3$. Using this effect, we realized THz near-field probes incorporating 3 μm apertures and we demonstrate transmission mode THz time-domain near-field imaging with spatial resolution of 3 μm, corresponding to λ/100 (at 1 THz). © *2014 Author(s). All article content, except where otherwise noted, is licensed under a Creative Commons Attribution 3.0 Unported License.*
[http://dx.doi.org/10.1063/1.4861621]

Terahertz (THz) spectroscopy and imaging is now applied widely in basic and applied research.[1] Due to the relatively large wavelength, spatial resolution beyond the diffraction limit in THz microscopy is achieved using near-field scanning probes.[2–9] The probe determines the spatial resolution as well as the nature of the detected signal. Sub-wavelength aperture probes and electro-optic probes so far have reached a spatial resolution of ~7–10 μm,[3–6] whereas scattering needle probes showed a spatial resolution better than 1 μm.[7,8] The contrast obtained by the scattering probes is a complex function of a number of parameters due to the local field enhancement produced by scattering probes and due to the probe dithering employed for these measurements.[6–8] The electro-optic and aperture probes on the other hand produce THz images, which typically correlate with the electric field distribution near the sample surface illuminated by a THz beam, showing the interaction of the THz wave with the sample directly. The sub-wavelength aperture probe, discussed here, in principle enables spatial resolution on the order of the aperture size, independent of the wavelength and over one order of magnitude better than the diffraction limit.[3] However, decreasing the aperture size (a) substantially below the wavelength (λ) is prohibitive because of the strong dependence of the transmitted wave amplitude on aperture size.[10]

According to Bethe's theory, the transmitted field amplitude (E) follows a a^3 power law (i.e., intensity $I \sim a^6$) for apertures $a \ll \lambda$.[11,12] This power law was confirmed experimentally at THz frequencies.[10] The limited transmission through these apertures has restricted the use of stand-alone apertures smaller than 20–30 μm for THz near-field microscopy. Each factor of 2 reduction in the aperture size produces a drop in the transmitted wave intensity by almost two orders of magnitude.

The problem of low transmission has been mitigated in integrated near-field probes, where a THz detector is placed in the near-field zone of the aperture.[3,5,13] The detector can sense evanescent field components, which dominate in the k-vector spectrum of the transmitted wave for small apertures ($a \ll \lambda$). However, even the evanescent field was observed to follow Bethe's a^3 dependence at a distance of 4 μm from the aperture.[10] It was recently pointed out that the strength of the THz evanescent field within 1–2 μm from the aperture deviates significantly from Bethe's dependence.[2,13] At this range, the electric field can be over an order of magnitude higher than what is expected from the a^3 dependence. In this Letter, we present THz near-field probes with a photo-conductive detector integrated within 1 μm from the aperture and we experimentally show that the sub-wavelength aperture transmission indeed deviates from Bethe's dependence of $E \propto a^3$. This effect not only allows us to use the integrated THz near-field probes with apertures as small as 3 μm for THz time-domain microscopy in transmission configuration, but also suggests an approach to reduce the aperture size further and to enable higher spatial resolution. We describe how the parameters of this aperture-type integrated near-field probe affect the probe sensitivity. We also demonstrate the highest spatial resolution (3 μm) achieved to date with an aperture-type near-field probe for THz time-domain spectroscopy and imaging.[2]

In the THz near-field probes with an integrated photoconductive detector, the minimal separation between the aperture screen and the detector antenna is limited first of all by the optical absorption length in the photoconductor and secondly by the requirement of electrical isolation between the aperture screen and the antenna. The optical absorption length in GaAs is ~1.4 μm at 800 nm and therefore a typical thickness of the photoconductive layer with sub-picosecond carrier lifetime is 1 μm. To ensure that there is no current leakage between the metallic screen and the contacts of the THz antenna, the probes must also contain a semiconductor (or dielectric) region, where no photo-carrier excitation can take place. The minimal separation between the aperture and the THz antenna has been ~4 μm (Ref. 3) and 2 μm (Ref. 14). This distance however is larger than the range of the strong evanescent field for apertures smaller than 3 μm. To

a)o.mitrofanov@ucl.ac.uk

 © Author(s) 2014

This article is copyrighted as indicated in the article. Reuse of AIP content is subject to the terms at: http://scitation.aip.org/termsconditions. Downloaded to IP: 144.82.107.68 On: Tue, 20 May 2014 14:15:49

take advantage of the evanescent field for such apertures, the entire THz detector must be sufficiently small to be accommodated within a short range ($\sim$1 μm) of the aperture.

To integrate the THz detector within 1 μm of the aperture, we modify the optical properties of the active region by incorporating a distributed Bragg reflector (DBR) between the aperture plane and a thinned photoconductive layer (Fig. 1(a)). The DBR has two main purposes. First, the photoconductive layer behaves like a low-Q cavity, leading to enhanced optical fields and increased carrier generation. Second, optical isolation prevents the gating optical pulse passing through the near-field probe and reaching the sample. This is important for imaging applications of this system as it permits imaging of light sensitive samples, such as semiconductor-based metamaterials, and reduces the effect of false contrast that can arise if the sample has non-uniform optical reflectivity. The proposed probe structure allows us to miniaturize the active region of the THz detector and to place it within 1 μm of the aperture.

The structure consists of a 505 nm thick, low-temperature grown (LT) GaAs active region, chosen as a multiple of $\lambda/4$ of the gating pulse wavelength (800 nm) to reinforce the DBR effect (Fig. 1(a)). The DBR is made up of 9 $\lambda/4$ layers of AlAs and $Al_{20\%}Ga_{80\%}As$. The DBR is separated from the metallic screen by a dielectric spacer layer made of either a combination of the 527 nm thick $Al_{20\%}Ga_{80\%}As$ layer and a 68 nm AlAs layer (both in multiples of $\lambda/4$), or a 30 nm thick Al_2O_3 film. The distance from the aperture plane to the antenna is therefore $\sim$1.6 μm and 1.0 μm, respectively, in the two designs.

A set of THz near-field probes with the antenna-aperture separation $z = 1.6$ μm and apertures of 3, 5, and 10 μm and a reference THz detector without the metallic screen are fabricated using the process described in Ref. 15. In summary, the samples are grown by molecular beam epitaxy (wafer number: VB0580). A THz antenna is deposited on the annealed LT GaAs surface using optical contact lithography. The antenna consists of two gold transmission lines and two pointed halves of a dipole antenna, separated by a gap $g = 7.5 \pm 1$ μm (Fig. 1(b)). Each antenna is transferred on to a sapphire substrate (with the antenna facing the substrate). After polishing away and etching the GaAs substrate, a 300 nm thick gold screen with a square aperture is deposited on the spacer layer. The aperture is aligned with the center of the antenna.

The combination of the DBR, the LT-GaAs layer and the spacer layer minimizes optical transmission of the gating pulse at the excitation wavelength. The optical transmission spectrum for the 1.6 μm-thick hetero-structure (mounted on a sapphire substrate and normalized to the substrate transmission coefficient) has a minimum of $<$10% near the excitation wavelength (800 nm). Periodic variation of the transmission coefficient shows the DBR effect (Fig. 1(c)).

For experimental evaluation of THz transmission through the probe aperture, THz pulses are generated using optical rectification in a 1.0 mm thick ZnTe crystal and coupled into a hollow cylindrical metallic waveguide, 1 mm in diameter and 80 mm in length (Fig. 1(d)). The waveguide is used in order to form an unfocused transverse THz wave with a well-defined beam profile ($\sim$0.5 mm intensity FWHM)[16] and to avoid the longitudinal electric field present in focused beams, which can be also detected by the probe.[17] The transparent substrate of the probe allows optical access to the photoconductive antenna for the optical gating pulses (mode-locked Ti:Sapphire laser, $\tau = 100$ fs, $\lambda = 800$ nm) focused on the antenna gap using a lens (NA = 0.5).

The waveform and the corresponding spectrum of the THz pulse detected using a 10 μm square aperture probe are shown in Fig. 2. Although the waveguide induces pulse broadening due to the waveguide dispersion and mode interference,[18] the transmission coefficient of the aperture can be evaluated using any shape of the THz pulse.

The amplitude of the detected THz field decreases by a factor of 5 for the 5 μm aperture compared to the 10 μm aperture, and by a factor of 40 for the 3 μm aperture. Their relative spectral amplitudes in the range of 1–1.5 THz are shown by blue symbols in Fig. 3. The functional dependence will be discussed later, however, here we note that the pulse waveform remains unchanged for all tested probes, despite the strong drop in amplitude. This observation agrees with the finding that the waveform of the transmitted THz pulse is independent of the aperture size in the regime $a < \lambda/10$ and the

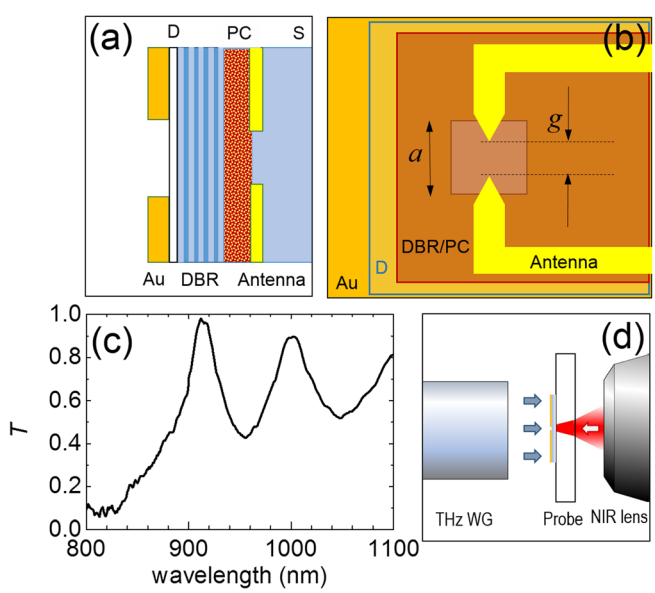

FIG. 1. Schematic cross-section (a) and diagram (b) of the integrated THz near-field probe: Au—gold screen with an aperture, D—insulating dielectric layer; DBR—distributed Bragg reflector, PC—photoconductive LT GaAs layer, S—sapphire substrate. (c) Optical transmission spectrum of the probe heterostructure (without the gold screen) normalized to the transmission through the sapphire substrate. (d) Schematic diagram of the experimental setup.

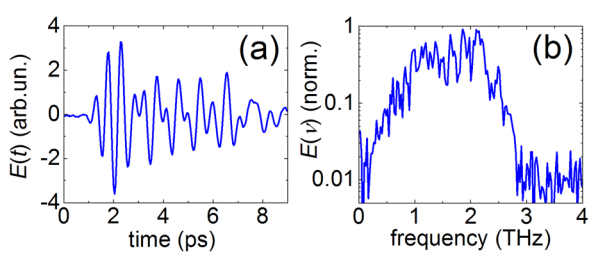

FIG. 2. THz pulses detected by a 10 μm aperture probe ($z = 1.6$ μm, $g = 7.5$ μm): (a) the time-domain waveform and (b) the amplitude spectrum (normalized to the peak value).

This article is copyrighted as indicated in the article. Reuse of AIP content is subject to the terms at: http://scitation.aip.org/termsconditions. Downloaded to IP: 144.82.107.68 On: Tue, 20 May 2014 14:15:49

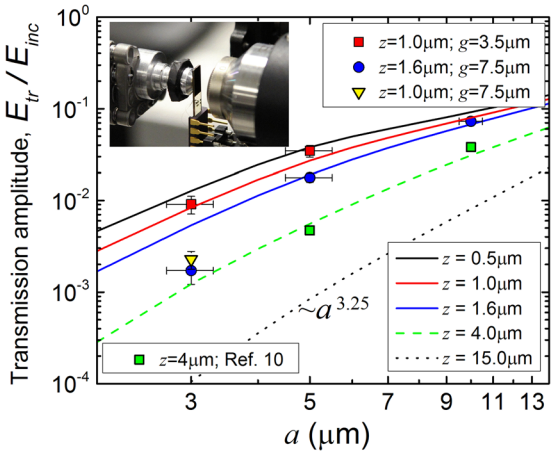

FIG. 3. Amplitude of the transmitted THz field. Symbols show the measurements at distances $z = 1\ \mu$m and 1.6 μm from the aperture of size a, and lines show numerical calculations at $z = 0.5$, 1, 1.6, 4, and 15 μm. The transmitted amplitude is calculated for the spectral range of 1–1.5 THz and normalized to the amplitude of the incident field. Green symbols show the transmitted amplitude data for $z = 4\ \mu$m from Ref. 10. *Inset:* a photographic image of the experimental setup showing the THz waveguide output, the probe and the focusing objective.

waveform corresponds to a temporal derivative of the incident wave.[19,20] Experimental evaluation of the relative transmission coefficient for probes with different aperture sizes is therefore possible not only in the frequency domain, but also in the time domain. The relative amplitude of the THz pulse time-domain waveforms allows us to evaluate the transmission coefficient for the 3 μm probe, for which the noise level becomes too high for performing Fourier analysis.

To investigate the impact of reducing the separation between the antenna and the aperture to $z = 1\ \mu$m, the 600 nm AlGaAs spacer is replaced by a 30 nm think Al_2O_3 layer. A 3 μm aperture probe with $z = 1\ \mu$m and a smaller gap between the dipole antenna tips ($3.5 \pm 0.5\ \mu$m) showed a factor of 10 improvement in the detected field amplitude. For a set of 3, 5, and 10 μm aperture probes with $z = 1\ \mu$m, the detected field follows a weaker dependence on aperture size than the a^3 power law predicted by Bethe's theory.

To analyze the functional dependence of the amplitude on aperture size, we compare the experimental results to the numerically computed amplitude of the electric field within a short distance of the apertures. We used a commercial solver based on the finite-difference time-domain method[21] to model THz pulse transmission through square holes in a 300 nm thick gold film placed on a GaAs substrate ($n = 3.59$). We select the range of 1–1.5 THz to match the experimental conditions used in this work, as well as a previous study of aperture transmission for comparison,[10] and plot the mean of the calculated transmission coefficient over this range. We also average the calculated E-field over a distance of 5 μm to evaluate the "average" field over the area of photo-excitation. It should be noted that the detector antenna is not included in the simulations.

In Fig. 3, the simulation results clearly show the benefits of moving the detector antenna close to the aperture. For $z = 15\ \mu$m, a dependence of slightly worse than a^3 is found. The extra losses beyond the Bethe model are associated with the finite thickness of the screen, which introduces waveguiding losses, and the Ohmic losses in the metal. For smaller z, the electric field amplitude increases significantly due to the evanescent nature of the transmitted field. We note that it is the aperture size, rather than the wavelength, that determines the distance at which the evanescent field remains strong. The wavelength determines whether the field is evanescent or propagating, however the aperture size determines the decay length of this field. The a^3 dependence persists for z significantly smaller than the wavelength. This result is consistent with the experimental results for near-field probes with the distance between the antenna and the aperture of $\sim 4\ \mu$m.[4] For even smaller z, however, the power law changes gradually towards a linear dependence $E \sim a^1$, found for $z = 0$ in the plane of the aperture,[13] and the amplitude of the field increases significantly.

In order to compare the simulation results to the experiments, the detected pulse amplitude must be normalized to the incident wave amplitude within the same frequency range. The incident field can be evaluated by a THz antenna detector without the metallic screen. In this case however the device response relative to simulations is enhanced by the antenna (Fig. 1) and a correction factor has to be applied. The physical reason for the correction factor is as follows. Without the aperture screen present, the incident E-field acts along the length of each antenna arm, leading to field enhancement at the antenna tips, which was observed in Ref. 22. When the aperture screen blocks a large fraction of the antenna, the incident E-field does not act along the whole antenna, but only at the antenna tips, and hence the enhancement effect is not present. If we assume that the antenna enhances the incident field by a factor of 4.1, we find a good match between the experiment and theory. Although it is difficult to determine a precise value of the enhancement factor because it depends on the antenna design[23] and on the size of the THz beam, the value of 4.1 is consistent with the antenna geometry. We also find a similar enhancement factor of 4.6 when comparing the earlier experimental study of the probes with $z = 4\ \mu$m (Ref. 10) with the present calculations. The value of the antenna enhancement factor and the transmission coefficient in Fig. 3 allows us to estimate the sensitivity of near-field probes relative to the photoconductive antenna detector. For example, the transmitted amplitude for a near-field probe with $a = 3\ \mu$m and $z = 1\ \mu$m is 0.009 (Fig. 3), whereas the antenna enhancement factor is 4.1. Therefore the sensitivity of the near-field probe is lower compared with the photoconductive antenna (without the aperture) by a factor of $0.009/4.1 = 0.0022$ (in amplitude) or by 53 dB (in power).

The functional dependences calculated for $z = 1.0\ \mu$m and for $z = 1.6\ \mu$m are followed by the experimental results closely except for the 3 μm probes with $g = 7.5\ \mu$m, for which the detected signal is noticeably weaker than predicted by calculations. This is attributed to the antenna tips being spaced further apart than the aperture size, meaning that the average field between the tips is reduced by approximately a factor of 2–3, consistent with the measured amplitude. This observation highlights the importance of scaling the photoconductive antenna gap with the aperture size in order to take advantage of the evanescent field, which is present only in the area of the aperture.

This article is copyrighted as indicated in the article. Reuse of AIP content is subject to the terms at: http://scitation.aip.org/termsconditions. Downloaded to IP: 144.82.107.68 On: Tue, 20 May 2014 14:15:49

These results show that by reducing the distance between the aperture and the detector we moved well beyond the Bethe dependence of $E \propto a^3$. This represents over one order of magnitude improvement for sensitivity of a near-field probe with this design. It allows us to detect THz waves through apertures as small as 3 μm. We note that the design discussed here was selected to enhance photo-carrier generation in the THz detector and to minimize transmission of the optical gating beam (800 nm) through the probe by introducing the DBR. However the design can be altered to increase the sensitivity of the near-field probes: for example, by optimizing the thickness of the active LT-GaAs layer and the number periods in the DBR. Optimization of the structure to take into account these effects should improve performance even further, leading to potential use of apertures as small as 1 μm.

Spatial resolution capabilities of the integrated near-field probes are evaluated by scanning an edge of a metallic strip deposited on GaAs in front of the 3 μm aperture probe. For this experiment we used an unfocused THz beam generated using the ZnTe crystal positioned approximately 5 mm away from the test sample (without a waveguide). The THz pulse waveform and the amplitude spectrum are shown in Fig. 4(a). The metallic edge is oriented parallel to the polarization. The amplitude of the THz pulse shows good contrast between the metallic and dielectric regions (Fig. 4(b), red line) with the transition region length of 3.3 ± 0.5 μm using the 10%–90% criterion or 2.5 μm using the 20%–80% criterion. This test confirms that the probe spatial resolution is determined by the aperture size.

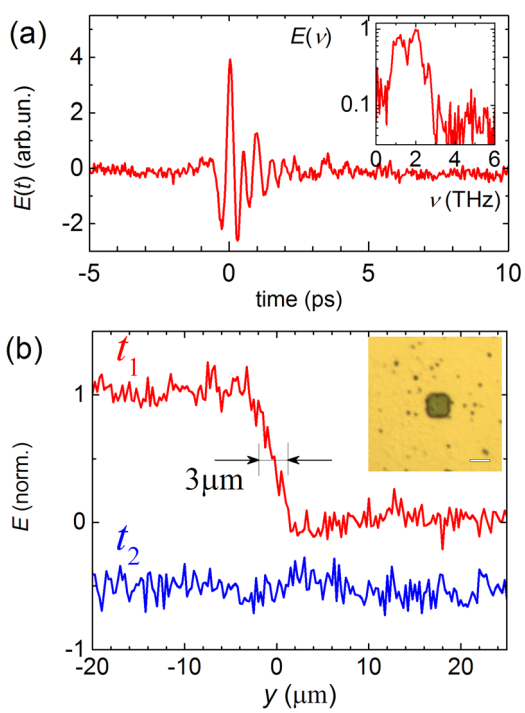

FIG. 4. (a) THz pulse waveform detected by a 3 μm aperture probe ($z = 1.0$ μm, $g = 3.5$ μm); *inset:* the pulse amplitude spectrum (normalized). (b) Normalized traces of the field amplitude, $E(t)$, detected by the probe when a metallic edge is scanned over the aperture: $t = t_1$ represents the detected field amplitude at the peak of the pulse and $t = t_2$ represents the field 2 ps prior the pulse arrival; *inset:* an optical image of the aperture (the scale bar is 3 μm).

To verify that the detected signal corresponds to the electric field of THz pulse, Fig. 4(b) also displays a trace (blue line) measured at the same location of the sample but 2 ps prior to the THz arrival. As expected, this trace shows no signal variation between the metallic and dielectric regions. We note that the probe is kept $\sim$1 μm from the sample during the scan. The probe sensitivity is not based on the local field enhancement effect and therefore it does not require dithering the probe or the sample, the method typically used in the scattering probe microscopy.

In conclusion, we have proposed and demonstrated an integrated photo-conductive probe for THz near-field microscopy in transmission, sensitive enough to use apertures as small as 3 μm ($\sim\lambda/100$ at 1 THz). The dependence of the probe sensitivity on aperture size is evaluated experimentally. It shows that the Bethe dependence of transmission through a single sub-wavelength aperture ($E \sim a^3$) weakens within the range of $\sim$1 μm of the aperture. This suggests that further improvements in resolution for the aperture-type probe are possible by optimising both the probe epilayer structure and the detector antenna design.

We would like to thank Professor Paul Planken for useful discussions of wave transmission through small apertures and gratefully acknowledge the support of the Royal Society [Grant No. UF080745]. This work was performed, in part, at the Center for Integrated Nanotechnologies, an Office of Science User Facility operated for the U.S. Department of Energy (DOE) Office of Science. Sandia National Laboratories is a multi-program laboratory managed and operated by Sandia Corporation, a wholly owned subsidiary of Lockheed Martin Corporation, for the U.S. Department of Energy's National Nuclear Security Administration under Contract No. DE-AC04-94AL85000.

[1]P. U. Jepsen, D. G. Cooke, and M. Koch, Laser Photonics Rev. **5**, 124 (2011).
[2]A. J. L. Adam, J. Infrared Millim. THz Waves **32**, 976 (2011).
[3]O. Mitrofanov, M. Lee, J. W. P. Hsu, I. Brener, R. Harel, J. Federici, J. D. Wynn, L. N. Pfeiffer, and K. W. West, IEEE J. Sel. Top. Quantum Electron. **7**, 600 (2001).
[4]F. Blanchard, A. Doi, T. Tanaka, and K. Tanaka, Annu. Rev. Mater. Res. **43**, 237 (2013).
[5]Y. Kawano and K. Ishibashi, Nat. Photonics **2**, 618 (2008).
[6]A. J. L. Adam, N. C. J. van der Valk, and P. C. M. Planken, J. Opt. Soc. Am. B **24**, 1080 (2007).
[7]K. Moon, Y. Do, M. Lim, G. Lee, H. Kang, K.-S. Park, and H. Han, Appl. Phys. Lett. **101**, 011109 (2012).
[8]T. L. Cocker, V. Jelic, M. Gupta, S. J. Molesky, J. A. J. Burgess, G. De Los Reyes, L. V. Titova, Y. Y. Tsui, M. R. Freeman, and F. A. Hegmann, Nat. Photonics **7**, 620 (2013).
[9]M. Wachter, M. Nagel, and H. Kurz, Appl. Phys. Lett. **95**, 041112 (2009).
[10]O. Mitrofanov, M. Lee, J. W. P. Hsu, L. N. Pfeifer, K. W. West, J. D. Wynn, and J. F. Federici, Appl. Phys. Lett. **79**, 907 (2001).
[11]H. Bethe, Phys. Rev. **66**, 163 (1944).
[12]C. J. Bouwkamp, Philips Res. Rep. **5**, 321 (1950).
[13]J. R. Knab, A. J. L. Adam, E. Shaner, H. J. A. J. Starmans, and P. C. M. Planken, Opt. Express **21**(1), 1101 (2013).
[14]M. Misra, Y. Pan, C. R. Williams, S. A. Maier, and S. R. Andrews, J. Appl. Phys. **113**, 193104 (2013).
[15]O. Mitrofanov, I. Brener, M. C. Wanke, R. R. Ruel, J. D. Wynn, A. J. Bruce, and J. Federici, Appl. Phys. Lett. **77**, 591 (2000).
[16]O. Mitrofanov, T. Tan, P. R. Mark, B. Bowden, and J. A. Harrington, Appl. Phys. Lett. **94**, 171104 (2009).
[17]R. Mueckstein and O. Mitrofanov, Opt. Express **19**, 3212 (2011).

This article is copyrighted as indicated in the article. Reuse of AIP content is subject to the terms at: http://scitation.aip.org/termsconditions. Downloaded to IP: 144.82.107.68 On: Tue, 20 May 2014 14:15:49

[18]M. Navarro-Cia, C. M. Bledt, M. S. Vitiello, H. E. Beere, D. A. Ritchie, J. A. Harrington, and O. Mitrofanov, J. Opt. Soc. Am. B **30**, 127 (2013).
[19]O. Mitrofanov, L. N. Pfeiffer, and K. W. West, Appl. Phys. Lett. **81**, 1579 (2002).
[20]A. J. L. Adam, J. M. Brok, M. A. Seo, K. J. Ahn, D. S. Kim, J. H. Kang, Q. H. Park, M. Nagel, and P. C. M. Planken, Opt. Express **16**, 7407 (2008).
[21]See http://www.lumerical.com/tcad-products/fdtd/ for Lumerical Solutions, Inc., Lumerical FDTD Solutions.
[22]P. U. Jepsen, R. H. Jacobsen, and S. R. Keiding, J. Opt. Soc. Am. B **13**, 2424 (1996).
[23]Y. Cai, I. Brener, J. Lopata, J. Wynn, L. Pfeiffer, and J. Federici, Appl. Phys. Lett. **71**, 2076 (1997).

This article is copyrighted as indicated in the article. Reuse of AIP content is subject to the terms at: http://scitation.aip.org/termsconditions. Downloaded to IP: 144.82.107.68 On: Tue, 20 May 2014 14:15:49